Batteries & Supercaps

Research Article
doi.org/10.1002/batt.202500430

Chemistry Europe
European Chemical Societies Publishing

www.batteries-supercaps.org

Safety Enhancement In Ni-Rich Nmc Lithium-Ion Batteries Through Lithium Manganese Iron Phosphate Additive Integration

Haiyang Zhang, Dewen Kong, Song Zhou, Jingyuan Liu, Yueqi Wang, Jinguo Miao, Lianghao Jia, Qingyu Dong, Haijing Liu,* Hui Shao,* Yanbin Shen,* and Liwei Chen

Increasing the nickel content in high-nickel ternary cathode materials enhances their specific capacity, thereby increasing the energy density of the battery. However, the elevation of nickel content often compromises both thermal stability and structural integrity, thereby, detracting from the safety performance of the battery and hindering the practical application of ultrahigh nickel content cathode materials. This study demonstrates that the addition of 10% $LiMn_{0.7}Fe_{0.3}PO_4$ (LMFP) does not significantly impair the electrochemical performance of $LiNi_{0.91}Co_{0.05}Mn_{0.03}Al_{0.01}O_2$ (NCMA) based batteries. Differential scanning calorimetry results demonstrate that the incorporation of 10% LMFP reduces the exothermic heat release from NCMA electrodes while enhancing the temperature of the exothermic peak. Furthermore, a variety of safety assessments conducted on pouch cell devices, including acupuncture, high-temperature chamber, and overcharge tests, confirm that the addition of 10% LMFP substantially enhances the safety of NCMA batteries. These findings highlight the potential of LMFP as a critical additive in overcoming the safety limitations associated with high-nickel cathode materials, thereby paving the way for the further development of safer high-energy-density battery systems.

1. Introduction

The proliferation and advancement of electric vehicles (EVs) have underscored the critical importance of battery energy density in extending driving range and meeting elevated performance demands.[1,2] Despite these advancements, EVs continue to grapple with "range anxiety"—a pervasive concern over insufficient battery endurance during prolonged use—thereby intensifying the urgent need for batteries with higher energy densities. Currently, ternary cathode materials ($LiNi_xM_{1-x}O_2$, where M = Mn, Co, Al, etc., and $x > 0.6$) have emerged as the predominant high-energy-density cathode materials.[3–5] These materials are favored for their superior specific capacity and energy density, making them the cornerstone of high-end power batteries. To further enhance battery energy density, researchers have proposed increasing the Ni content ($Ni > 0.9$) within these ternary materials.[6–8] However, this approach introduces a series of formidable challenges.

The migration barrier for Ni ions is significantly lower compared to Co, Mn, and Al. Consequently, as the Ni content increases, the phase transition temperature of layered ternary materials markedly decreases. Notably, when the Ni content surpasses 90%, the exothermic reactions can be triggered at temperatures below 190 °C, releasing up to 1000 J g^{-1} of heat.[9–11] This substantial heat generation severely limits the applicability of high-nickel ternary materials in energy storage systems. Moreover, elevated Ni content leads to an increased proportion of high-valence Ni ions (e.g., Ni^{3+}, Ni^{4+}), which destabilize the crystal structure, particularly inducing irreversible phase transitions within the layered architecture.[12] This phase transformation is accompanied by oxygen release and additional heat generation, further exacerbating material instability.[13] The resultant heat and oxygen can precipitate a cascade of safety hazards, including separator failure, electrolyte combustion, and exothermic reactions at the anode, ultimately culminating in thermal runaway and compromising overall battery safety. Thus, despite the pronounced advantages of high-nickel ternary materials in energy density, the concomitant safety concerns substantially hinder their widespread adoption in high-performance batteries. Existing mitigation strategies, such as surface coating techniques

H. Zhang, S. Zhou, Y. Wang, L. Jia, Q. Dong, H. Shao, Y. Shen
i-lab
Suzhou Institute of Nano-Tech and Nano-Bionics
Chinese Academy of Sciences
Suzhou, Jiangsu 215123, China
E-mail: hshao2023@sinano.ac.cn
ybshen2017@sinano.ac.cn

D. Kong, J. Liu, H. Liu
Battery Research and Development Laboratory
Battery Propulsion & Sustainability, General Motors
Shanghai 201206, China
E-mail: Helen.liu@gm.com

J. Miao, Y. Shen
KnowLitech Inc. Ltd.
Shaoxing, Zhejiang 312000, China

L. Chen
In-situ Center for Physical Sciences
School of Chemistry and Chemical Enginerring
Shanghai Jiao Tong University
Shanghai 200240, China

Supporting information for this article is available on the WWW under https://doi.org/10.1002/batt.202500430

and flame-retardant electrolytes, have been employed to enhance the safety of high-nickel ternary materials.[14,15] However, these methods often incur a tradeoff by diminishing electrochemical performance. Recent study by Hong et al. has demonstrated that incorporating $LiMn_{0.7}Fe_{0.3}PO_4$ (LMFP) nanoparticles into the high-nickel ternary cathode material $LiNi_{0.6}Co_{0.2}Mn_{0.2}O_2$ (NCM622) markedly improves material safety without adversely affecting its electrochemical properties.[16] LMFP effectively blocks direct contact between the high-nickel ternary material and the electrolyte, thereby delaying oxygen release and heat generation at elevated temperatures, which significantly enhances the material's thermal stability.[17–20] Additionally, LMFP mitigates the dissolution and deposition of transition metals (Ni, Co, Mn), further augmenting the battery's cycle life and safety. However, for high-nickel ternary materials with Ni content as high as 90%, both thermal and structural stability pose even more severe challenges.[21,22] To date, there has been no reported research on whether LMFP particles can further enhance the safety performance of such ultrahigh-nickel materials.

In this study, we introduce LMFP into $LiNi_{0.91}Co_{0.05}Mn_{0.03}Al_{0.01}O_2$ (NCMA) electrodes to investigate its efficacy in improving the safety performance of high-nickel ternary electrodes. Differential scanning calorimetry (DSC) analyses reveal that LMFP significantly enhances the thermal stability of NCMA materials. Further investigations indicate that both 10% and 25% LMFP additions yield comparable improvements in the safety performance of NCMA, with the 10% addition exerting a minimal impact on the electrochemical performance. We fabricated soft-pack cells using NCMA electrodes with a 10% LMFP addition and subjected them to a series of safety tests, including piercing, overcharging, and high-temperature thermal runaway. The results unequivocally demonstrate that LMFP incorporation substantially enhances the safety performance of NCMA electrodes, offering a promising pathway for the deployment of high-energy-density, high-nickel cathode materials in next-generation EV batteries.

2. Results and Discussions

In this study, commercially procured high-pressure, high-density polycrystalline NCMA material was utilized as the model system to investigate the effects of LMFP nanoparticle incorporation on the structural and thermal stability of high-nickel ternary cathodes. Figure S1, Supporting Information, displays the typical morphological structure of the NCMA material, which consists of secondary particle agglomerates with sizes ranging from 2 to 10 μm. Initially, NCMA/LMFP slurries were prepared by introducing varying mass percentages of LMFP slurry into the polycrystalline NCMA material during the mixing process. The LMFP slurry was obtained by predispersing LMFP nanoparticles in N-methyl-2-pyrrolidone (NMP) solvent, achieving a solid content of ≈40%. These slurries were subsequently processed using conventional electrode fabrication techniques to produce mixed electrodes with LMFP mass fractions of 10% and 25%, designated as NCMA-10 and NCMA-25, respectively.

Scanning electron microscopy (SEM) was employed to examine the morphology of the NCMA, NCMA-10, and NCMA-25 electrodes, with images captured from both top and cross-sectional views, as illustrated in **Figure 1**. Pure NCMA electrodes exhibit significant voids between active material particles, which are predominantly filled with conductive carbon black (Figure 1c). Upon the addition of 10% LMFP, the LMFP nanoparticles form a dense coating around the NCMA particles, and the mixture of LMFP and conductive carbon black uniformly fills the interparticle voids, resulting in a highly homogeneous and compact electrode structure (Figure 1f). However, when the LMFP content is increased to 25%, noticeable gaps emerge between the LMFP and NCMA particles (Figure 1i). This phenomenon is likely attributable to the higher specific surface area (20 $m^2 g^{-1}$) of LMFP, which, at elevated mass fractions, may compromise the adhesive strength of the binder, leading to incomplete filling of interparticle spaces.

To evaluate the electrochemical behavior of the three NCMA electrode variants and pure LMFP electrodes, coin cell half-cells were assembled and subjected to charge–discharge cycling at a 0.1C rate. **Figure 2**a presents the first cycle charge–discharge curves, revealing that the pure NCMA and pure LMFP electrodes exhibit discharge capacities of 210.2 and 149.1 mAh g^{-1}, respectively. The incorporation of LMFP into the NCMA electrodes results in a reduction of discharge capacity, with the NCMA-10 and NCMA-25 electrodes delivering discharge capacities of 202.8 and 197.4 mAh g^{-1}, respectively.

To assess the influence of LMFP additives on the thermal safety of NCMA electrodes, DSC was conducted on fully charged NCMA, NCMA-10, and NCMA-25 electrodes (Figure S1, Supporting Information). As shown in Figure 2b, pure NCMA begins to exhibit exothermic reactions at ≈190 °C, with a prominent exothermic peak at 203 °C and an associated heat release of up to 929 J $g.^{-1}$.[23] An exothermic peak is observed at 273 °C for the bare LMFP electrode, corresponding to a heat release amount of 91.5 J g^{-1}. For NMCA-10 electrode, the addition of 10% LMFP elevates the exothermic peak temperature by 10.8 °C and reduces the heat release to 218 J g^{-1}. These DSC results indicate that the LMFP additive significantly mitigates the exothermic heat generation of NCMA, thereby lowering the risk of thermal runaway in ultra-high-nickel-content NCMA materials. This result can be attributed to the poor thermal conductivity and good thermal stability of LMFP.[24] When LMFP nanoparticles are coated on the surface of NMCA, they can form an effective protective layer, which can effectively reduce heat transfer and improve the thermal stability of the complex.[25] Increasing the LMFP content to 25% further decreases the heat release to 155 J g^{-1}. However, this reduction is not significant compared to the 10% LMFP addition. Additionally, the 25% LMFP additive results in a lower discharge capacity and greater polarization, as evidenced by both the DSC data and electrochemical performance metrics. Therefore, a 10% LMFP additive is deemed optimal for enhancing safety without markedly compromising the electrochemical properties of NCMA.

Electrochemical impedance spectroscopy (EIS) Nyquist plots of NCMA and NCMA-10 pouch cells were tested and presented in Figure 2d. The introduction of LMFP additives elevates total cell impedance by ≈5 mΩ (20% increase relative to baseline). This

Research Article
doi.org/10.1002/batt.202500430
Chemistry Europe
European Chemical Societies Publishing

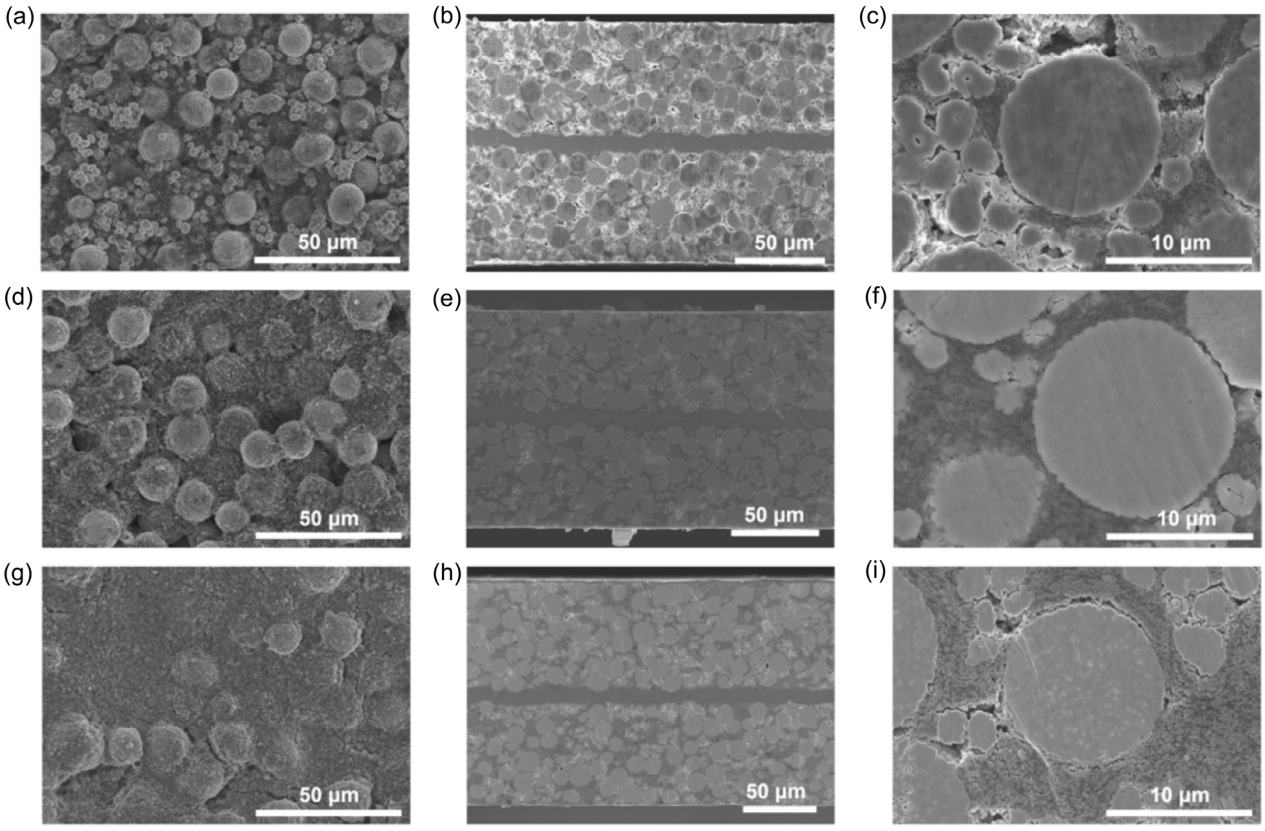

Figure 1. Top view and cross-section morphology of a–c) NCMA, d–f) NCMA-10, and g–i) NCMA-25 electrodes, respectively.

impedance increase is attributed to the inherently poor intrinsic ionic conductivity and electronic conductivity of the LMFP material. To further evaluate the electrochemical performance impact of LMFP doping, 1 Ah pouch cells were fabricated using commercially available graphite as the anode and either pure NCMA or NCMA-10 as the cathode. Figure 2e illustrates the rate performance tests conducted across 0.1C to 3C rates. The results indicate a slight decline in rate performance upon LMFP addition, which can be attributed to the inherent lower rate capability of LMFP materials. Subsequent long-term cycling at 0.33C (Figure 2e) revealed that both pure NCMA and NCMA-10 cells maintained nearly identical capacity retention after 500 cycles, demonstrating that LMFP additives do not detrimentally affect the cycling stability of NCMA.

Safety assessments were performed on these pouch cells by subjecting to acupuncture, high-temperature thermal runaway, and overcharging tests. Precharged NCMA cells (4.0 V, corresponds to a state of charge around 75%) exhibited immediate short-circuiting upon piercing, with voltages plummeting to 0 V and temperatures soaring to 323 °C, culminating in thermal runaway and intense combustion (**Figure 3**a and SVideo 1, Supporting Information). In stark contrast, NCMA-10 cells demonstrated only a minor voltage drop of 0.2 V postpiercing at an elevated charging voltage of 4.2 V, with no significant temperature increase or thermal runaway observed (Figure 3b and SVideo 2, Supporting Information). During the nail penetration in NCMA pouch cell, a short circuit occurs between the anode and cathode, leading to instantaneous discharge and a rapid voltage drop. The rapid heat generation stemming from the high current causes structural phase transitions in NCMA materials, a process accompanied by the release of oxygen and heat, ultimately resulting in thermal runaway and igniting the electrolyte.[26] Upon the addition of LMFP, this compound fills the surfaces and interstices of the ternary particles. Notably, LMFP exhibits inferior electrical and ionic conductivity compared to ternary materials, which does not significantly affect electrochemical performance under conditions such as 3C rates. However, during a short circuit, the local instantaneous current density can reach hundreds of degree. Under such extreme rates, the poor electrical and ionic conductivity of LMFP particles contributes positively by serving as an effective resistor, thereby delaying the extreme reactions of ternary particles at the penetration site during short circuit events. This resistance effectively suppresses the onset of the thermal runaway chain reaction. It is worth mentioning that the thermal stability of the NCMA material deteriorates progressively at deeper delithiation states. The NCMA-10 cell containing 10% LMFP additive demonstrated exceptional safety performance during nail penetration tests under higher delithiation states, further affirming the reliability of our additive approach.

Further investigations were conducted through thermal runaway tests within a high-temperature chamber on these two pouch cells precharged to 4.0 V, aimed at exploring the impact of LMFP on improving the thermal stability of NCMA.[27] As shown in Figure 3c, thermal runaway in the NCMA pouch cell occurred at

Research Article
doi.org/10.1002/batt.202500430
Chemistry Europe
European Chemical Societies Publishing

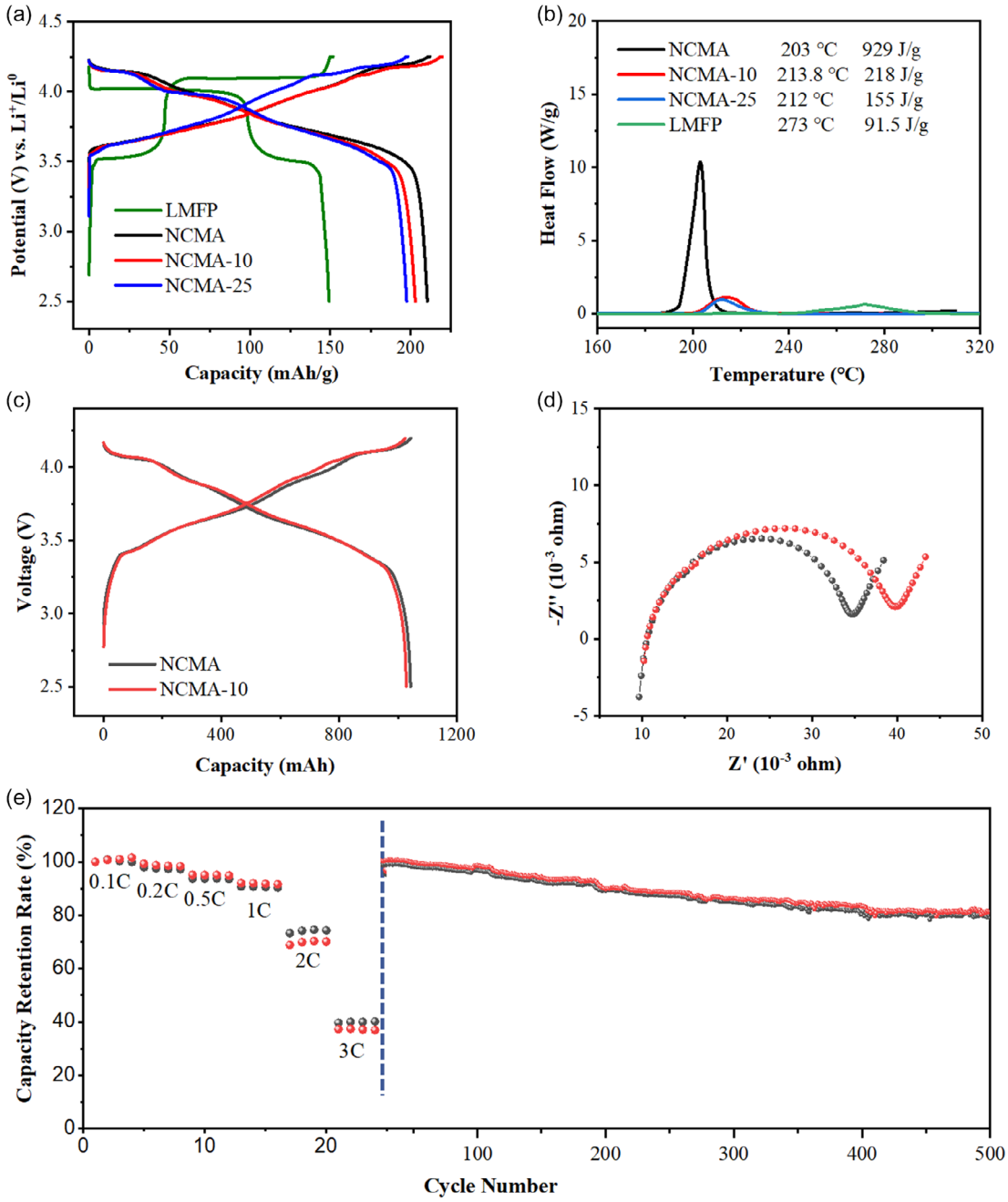

Figure 2. a) Charge/discharge curves of NCMA, LMFP, NCMA-10, and NCMA-25 electrodes tested by coin cells. b) DSC results of NCMA, LMFP, NCMA-10, and NCMA-25 electrodes at fully charged state. c) Charge/discharge curves and d) EIS Nyquist plots of NCMA and NCMA-10, tested with full cell configuration (pouch cell) paired with graphite as the anode. e) Rate performance and cycle performance of NCMA and NCMA-10 pouch cell.

a temperature of 186.1 °C, whereas the NCMA-10 pouch cell exhibited thermal runaway at 196.3 °C, indicating an increase in thermal runaway temperature of 10.2 °C. It is noteworthy that the enhancement in thermal runaway temperature of NCMA after the addition of LMFP aligns with the previous results obtained from the DSC analysis.[28,29] As noted earlier, the LMFP protective layer on the surfaces of NCMA particles in the NCMA-10 electrode can reduce thermal conductivity, while the excellent thermal stability of LMFP effectively enhances the thermal stability of the composite electrode. Moreover, the incorporation of LMFP has also improved the overcharge performance of NCMA-based batteries. As depicted in Figure 3d, upon the addition of 10% LMFP, the maximum voltage of NCMA-based batteries under identical overcharge test conditions increased from 5.22 V for pure NCMA to 5.75 V for NCMA-10. The enhancement in overcharge capability may be attributed to the LMFP coating on the surfaces of NCMA particles, which reduces direct contact with the electrolyte, thereby diminishing side reactions at the interface of active materials and the electrolyte under high voltage, and thus improving overcharge performance.

Research Article
doi.org/10.1002/batt.202500430
Chemistry Europe
European Chemical Societies Publishing

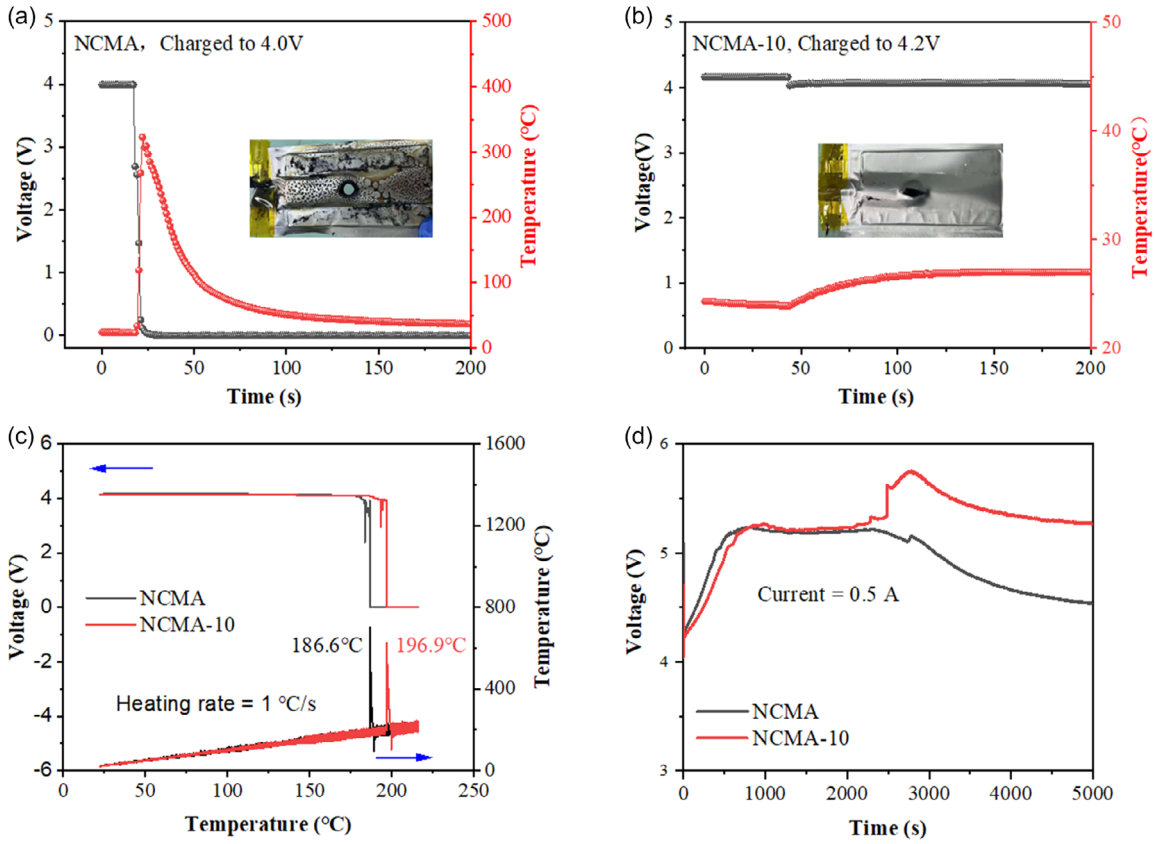

Figure 3. Safety test experiments based on pouch cells. a–b) acupuncture tests, c) high-temperature chamber tests, and d) overcharge tests.

3. Conclusion

In conclusion, this study demonstrates that the incorporation of LMFP significantly enhances the safety of batteries utilizing ternary cathode materials with an ultrahigh Ni content of 90%. DSC results reveal that the addition of 10% LMFP effectively reduces the exothermic heat release from the NCMA electrodes while simultaneously elevating the temperature of the exothermic peak. A comprehensive series of electrochemical tests further indicate that this level of LMFP addition does not adversely affect the electrochemical performance of NCMA-based batteries. Encouragingly, a variety of safety assessments performed on pouch cell devices, including puncture, overcharge, and high-temperature chamber, illustrate that the 10% addition of LMFP significantly improves the safety profile of NCMA-based batteries. These findings underscore the feasibility of utilizing LMFP as a protective additive in NCMA cathodes, providing a promising pathway for enhancing the overall safety of high-energy-density lithium-ion batteries.

4. Experimental Section

Materials Preparation

High-nickel cathode materials ($LiNi_{0.91}Co_{0.05}Mn_{0.03}Al_{0.01}O_2$, denoted as NCMA) were supplied by CNGR Advanced Material Co. Ltd. Lithium manganese iron phosphate ($LiMn_{0.7}Fe_{0.3}PO_4$, LMFP) was provided by KnowLitech Inc. Ltd. (Shaoxing, China). Figure S5, Supporting Information, presents the morphology of the LMFP powder, showing that its primary particle size is ranges from 100 to 200 nm. The anode material was SMA-B graphite (BTR New Material Group). Conductive additives included Super P (Imerys) and multiwalled carbon nanotubes (CNT, CN-1N slurry, Cnano Technology). Binders for cathodes and anodes were PVDF-5130 (Solvay) and a mixture of NV-1T/CMC (Nippon Shokubai), respectively. The electrolyte formulation for both coin and pouch cells consisted of 1 m $LiPF_6$ in ethylene carbonate/ethyl methyl carbonate (EC/EMC, 7:3 v/v) with 1% vinylene carbonate (VC) and 2% fluoroethylene carbonate (FEC).

Cell Fabrication: Coin Cells

Cathode slurries were prepared in a dry room (dew point ≤ -40 °C) by blending active materials (NCMA or NCMA-10, where NCMA-10 denotes 90 wt% NCMA + 10 wt% LMFP), Super P (2.9 wt%), CNT slurry (0.1 wt%), and PVDF (2 wt%) in N-methyl-2-pyrrolidone (NMP). Solid contents were adjusted to 65% and 60% for NCMA and NCMA-10 slurries, respectively. The homogenized slurry was coated onto aluminum foil using a doctor blade, dried at 80 °C for 12 hr, and punched into 12-mm-diameter discs. Electrodes were vacuum-dried at 100 °C for >48 h before cell assembly.

Cell Fabrication: Pouch Cells

Cathodes (34 × 63 mm) and anodes (35 × 64 mm) were fabricated with identical compositions to coin cells but scaled to 4 and

4.4 mAh cm^2 areal capacities, respectively. The negative-to-positive capacity ratio (N/P) was set to 1.1. Six cathode sheets and seven anode sheets were stacked with double-sided Al_2O_3-coated PE separators (12 μm base with 2 μm Al_2O_3 coating per side). Cells were vacuum-sealed after electrolyte filling (2.5 g Ah^{-1}) and aged for 48 hr at 25 °C.

Material Characterization

Electrode morphology was analyzed via field-emission SEM (Hitachi SU8200, 10 kV). Cross-sectional samples were prepared using argon ion milling (Gatan 697, 5 kV, 6 h, −60 °C). Thermal stability of delithiated cathodes was assessed by DSC (TA DSC-250) at 5 °C min^{-1} from 30 to 350 °C using 1:0.3 (w/w) electrode/electrolyte mixtures in sealed high-pressure crucibles.

Electrochemical Testing

Coin cells (CR2025) were assembled with lithium metal counte.

Electrochemical Testing: Thermal Runaway

Cells were heated at 1 °C min^{-1} in an environmental chamber with temperature probes attached to cell surfaces.

Electrochemical Testing: Overcharge

Cells were charged to 6 V at 0.5 A under temperature surveillance.r electrodes and tested between 2.5 and 4.25 V on a NEWARE CT-4000 system. Cyclic voltammetry (0.1 mV s^{-1}) was performed using a BioLogic VMP3 workstation. Pouch cells (1 Ah capacity) underwent rate capability tests (0.1C–3C, 1C = 1 A) and long-term cycling at 0.33C. EIS was tested on Biologic V300 rang from 200 KHz to 0.1 Hz after 3 cycles.

Safety Testing: Nail Penetration

Fully charged cells were pierced with a 5 mm steel needle at 25 mm s^{-1} while monitoring voltage and surface temperature.

Acknowledgements

H.Z. and D.K. contributed equally to his work. This work was financially supported by the National Natural Science Foundation of China (Grant nos. 22179143 and 22309202), and the Gusu Leading Talents Program (Grant no. ZXL2023190). The authors also acknowledge the technical support for Nano-X from Suzhou Institute of Nano-Tech and Nano-Bionics, Chinese Academy of Sciences (SINANO).

Conflict of Interest

The authors declare no conflict of interest.

Data Availability Statement

The data that support the findings of this study are available from the corresponding author upon reasonable request.

Keywords: additive · $LiMn_{0.7}Fe_{0.3}PO_4$ · safety performance · ultrahigh nickel content cathode materials

[1] G. Crabtree, *Science* **2019**, *366*, 6464.
[2] S. Zhang, X. Zhu, Z. Wang, L. Wang, Z. Zhang, Y. Liu, H. Z. J.Qiu, X. He, *Batt. Supercaps* **2025**, *8*, e202400355.
[3] W. Lee, S. Muhammad, C. H. Sergey, H. Lee, J. Yoon, Y. Kang, W. Yoon, *Angew. Chem., Int. Ed.* **2020**, *59*, 2578.
[4] F. Wang, J. Bai, *Batt. Supercaps* **2022**, *5*, e202100174.
[5] T. Dong, S. Zhang, Z. Ren, L. Huang, G. Xu, T. Liu, S. Wang, G. Cui, *Adv. Sci.* **2023**, *11*, 2305753.
[6] T. Yang, K. Zhang, Y. Zuo, J. Song, Y. Yang, C. Gao, T. Chen, H. Wang, W. Xiao, Z. Jiang, D. Xia, *Nat. Sustain.* **2024**, *7*, 1204.
[7] J. Hu, H. Wang, B. Xiao, P. Liu, T. Huang, Y. Li, X. Ren, Q. Zhang, J. Liu, X. Ouyang, X. Sun, *Natl. Sci. Rev.* **2023**, *10*, 252.
[8] J. Yang, X. Liang, H. Ryu, C. Yoon, Y. Sun, *Energy Storage Mater.* **2023**, *63*, 102969.
[9] B. Cui, Z. Xiao, S. Cui, S. Liu, X. Gao, G. Li, *Electrochem. Energy Rev.* **2024**, *7*, 27.
[10] D. Wang, L. Zheng, X. Li, G. Du, Y. Feng, L. J. Z. Da, *Int. J. Energy Res.* **2020**, *44*, 12158.
[11] H. Wang, W. Shi, F. Hu, Y. Wang, X. Hu, H. Li, *Energy* **2021**, *224*, 120072.
[12] H. Xie, H. Peng, D. Jiang, Z. Xiao, X. Liu, H. Liang, M. Wu, D. Liu, Y. Li, Y. Sun, S. Zhong, Z. Qian, R. Wang, *Chem. Eng. J.* **2023**, *470*, 144051.
[13] L. Jia, D. Wang, T. Yin, X. Li, L. Li, Z. Dai, L. Zheng, *ACS Omega* **2022**, *7*, 14562.
[14] Z. Cui, A. Manthiram, *Angew. Chem. Int. Ed.* **2023**, *135*, e202307243.
[15] G. Wei, R. Huang, G. Zhang, B. Jiang, J. Zhu, Y. Guo, G. Han, X. Wei, H. Dai, *Appl. Ener.* **2023**, *349*, 121651.
[16] Z. Hong, H. Dong, S. Han, W. Li, Q. Dong, Y. Cao, X. Gao, W. L. Yi. Zhang, L. Chen, *J. Power Sources* **2021**, *512*, 230505.
[17] L. Wen, Y. Shi, L. Ye, C. Wang, F. Li, *Mater. Sci. Eng. R Rep.* **2025**, *164*, 100952.
[18] S. Baek, J. Roh, J. Pyun, Y. Lee, S. Lee, S. Hong, N. Kim, M. S. Chae, *Batt. Supercaps* **2025**, *1*, e202500207.
[19] Y. Wu, Z. Zeng, M. Liu, C. Cai, S. Lei, H. Zhang, S. Cheng, J. Xie, *Adv. Energy Mater.* **2024**, *14*, 2401037.
[20] L. Wang, R. Wang, C. Zhong, L. Lua, D. Gong, Y. F. Qi. Shi, X. Wang, C. Zhan, G. Liu, *J. Energy Chem.* **2022**, *72*, 265.
[21] Y. Duan, S. Chen, L. Zhang, L. Guo, F. Shi, *Energy Fuels* **2024**, *38*, 5607.
[22] G. Park, B. Namkoong, S. Kim, J. Liu, C. Yoon, Y. Sun, *Nat. Ener.* **2022**, *7*, 946.
[23] Z. Xiao, P. Liu, Z. C. Li. Song, J. Du, C. Zhou, P. Jiang, *Ionics (Kiel).* **2021**, *27*, 3207.
[24] B. Zhang, X. Xie, Z. Peng, G. Hu, K. Du, B. Makuza, Y. Gong, X. Ji, Y. Cao, *J. Power Sources* **2022**, *541*, 231671.
[25] D. Ouyang, Y. Liu, I. Hamam, J. Wang, J. Dahn, *J. Energy Chem.* **2021**, *60*, 523.
[26] J. Xu, W. Mei, C. Zhao, Y. Liu, L. Zhang, Q. Wang, *J. Therm. Anal. Calorim.* **2021**, *144*, 273.
[27] Y. Sun, *ACS Energy Lett.* **2022**, *7*, 1774.
[28] S. Sharma, S. Pandey, T. Gusain, P. Gautam, R. Mishra, A. Hussain, S. Kumar, *J. Stor. Prod. Res.* **2024**, *109*, 102416.
[29] B. C. Koenig, P. Zhao, S. Deng, *J. Power Sources* **2023**, *581*, 233443.

Manuscript received: June 3, 2025
Revised manuscript received: July 28, 2025
Version of record online: